Magnetically induced Schrödinger cat states: The shadow of a quantum space

Partha Nandi [1,2,*] Nandita Debnath [3,4,†] Subhajit Kala [5,‡] and A. S. Majumdar[6,§]

[1]*Department of Physics, University of Stellenbosch, Stellenbosch 7600, South Africa*
[2]*National Institute for Theoretical and Computational Sciences (NITheCS), Stellenbosch, 7604, South Africa*
[3]*Department of Physics, University of Calcutta, Kolkata 700009, India*
[4]*School of Physical Sciences, Indian Association for the Cultivation of Science, Kolkata 700032, India*
[5]*Department of Physics, Indian Institute of Technology Guwahati, Guwahati 781039, Assam, India*
[6]*S. N. Bose National Centre for Basic Sciences, Salt Lake, Kolkata 700106, India*

Schrödinger cat states, which are superpositions of macroscopically distinct states, are potentially critical resources for upcoming quantum information technologies. In this paper we introduce a scheme to generate entangled Schrödinger cat states in a nonrelativistic electric dipole system situated on a two-dimensional plane, along with an external potential and a uniform strong magnetic field perpendicular to the plane. Additionally, our findings demonstrate that this setup can lead to the phenomenon of collapse and revival of entanglement for a specific range of our model parameters.

I. INTRODUCTION

In quantum theory, the transition between the microscopic and macroscopic worlds is one of the less understood features [1]. Such a transition plays a direct role in the realm of quantum measurements. In an ideal measurement paradigm, the interaction of macroscopic equipment and a microscopic system yields entanglement and a superposed quantum state with both macroscopic and microscopic components [2]. Schrödinger was the first to highlight the physical subtleties of this kind of superposition by replacing the macroscopic part of the system by a "cat" in order to illustrate a dramatic superposition of "states" of both alive and dead cats that should, in practice, be distinguished macroscopically [3]. The superposition of macroscopically different quantum states, generically referred to as the nonclassical Schrödinger cat state (SCS) [3–5], is crucial for understanding the conceptual underpinnings of quantum physics, especially with reference to wave-function collapse models [6–9]. In recent years, the advancement of quantum technologies has brought into sharp focus the utility of several quantum phenomena such as photon antibunching [10], sub-Poissonian statistics [11], and squeezing [12], along with the dynamics of the SCS.

The success of quantum information theory and its potential applications [13,14] that significantly outperform their classical equivalents have recently sparked a renewed interest in the generation of nonclassical states such as the SCS. Several applications of cat states have been suggested in the realm of quantum information [15], quantum metrology [16], quantum teleportation [17], and quantum error correction schemes [18,19]. In addition, the concept of decoherence between two superposed quantum objects, or the quantum-to-classical transition, can be studied using the SCS as a platform. In quantum optics, a superposition of two diametrically opposite coherent states $|\pm\alpha\rangle$, with a large value of $|\alpha|$, can be interpreted as a quantum superposition of two macroscopically distinct states, i.e., a Schrödinger catlike state [20,21]. However, due to decay of their interference properties, it is extremely difficult to detect such states in practice [22]. Nonetheless, the universality of the SCS enables it to be realized in a wide variety of physical arenas such as nonlinear quantum optics [23], quantum-dot systems [24], superconducting cavities [25], Bose-Einstein condensates [26], and quantization of weak gravity [27–29]. A fascinating direction of research in recent years has been the mechanism for the natural generation of the SCS in some specific condensed-matter systems [30,31].

Schrödinger cat states with entanglement-based protocols provide a novel technique to explore short-distance quantum physics in a nonrelativistic domain when there is a magnetic dipole interaction background [32]. At extremely short distances, the space-time structure needs to be granular in order to account for both gravity and quantum uncertainty [33]. A viable approach towards quantum gravity is through quantizing space-time itself [34], rather than the construction of an effective-field theory of gravity. This approach is an active area of research on quantum gravity, commonly referred to as noncommutative geometry [35,36]. The fundamental goal is to derive classical geometry from a suitable limit of a noncommutative algebra. Though such a proposal may appear as *ad hoc* [37], the physical justification for such a noncommutative space-time is strong since it provides a solution to the geometric measurement problem near the Planck scale.

Noncommutative geometry appears naturally in various nonrelativistic planar systems. For instance, it occurs using the lowest-Landau-level projection to study the behavior of charged particles in a strong magnetic field [38]. Further, the incompressibility of fractional quantum Hall fluids [39] has

---

*Contact author: pnandi@sun.ac.za
†Contact author: debnathnandita14@gmail.com; spsnd3125@iacs.res.in
‡Contact author: s.kala@iitg.ac.in
§Contact author: archan@bose.res.in

a strong connection to the emergence of a noncommutative geometry in which the fundamental Planck length is replaced by the magnetic length. Noncommutative space-time forms an alternative paradigm for studying the behavior of relativistic anyonic systems interacting with the ambient electromagnetic field [40,41]. Additionally, noncommutative properties of real-space coordinates in the presence of the Berry curvature [42] produce skew scattering by a nonmagnetic impurity without relativistic spin-orbit interactions in a condensed-matter system. Noncommutative space provides a paradigm for describing the behavior of the quantum-to-classical transition under the influence of decoherence [43,44], which is relevant for implementation of quantum information protocols. From an experimental standpoint, there have been efforts in search of evidence of possible noncommutative effect manifestations in cosmology and high-energy physics [45–47]. A testable framework has been suggested in low-energy experiments in the arena of the quantum Hall effect [48,49].

The motivation for the present study is to investigate whether a multicomponent entangled nonclassical SCS could be produced in deformed quantum space, where noncommutativity arises naturally in an easily accessibly low-energy physical system. In this article we investigate the phenomenology of a two-particle electric dipole model with an additional harmonic interaction and a strong background magnetic field, with motion constrained to the plane perpendicular to the field. Such a system may be considered as a toy version of a real excitonic dipole setup [50]. By exploring the high magnetic-field limit, we reveal the emergence of planar noncommutative space as a natural consequence. Furthermore, we establish the deformed Heisenberg algebra as the origin of the multicomponent entangled SCS in this system. Moreover, we quantify the degree of entanglement of our SCS and show that the phenomenon of collapse and revival of entanglement [51–53] occurs in this system under the influence of the harmonic potential.

The organization of our paper is as follows. The interacting two-particle electric dipole system is introduced in Sec. II, showing how classical noncommutative space appears in the presence of a very strong, constant, uniform magnetic field. In Sec. III we move on to the quantum picture, where intricacies of the system dynamics are revealed in the context of mapping between two reference frames. Section IV discusses how our model with a harmonic-oscillator potential that is dependent only on one spatial variable is able to generate entangled multicomponent Schrödinger cat states. In Sec. V we compute the degree of entanglement in the generated SCS system and demonstrate that it exhibits the phenomenon of entanglement collapse and revival. Section VI provides a summary and discussion of our results. Appendix A discusses the phase-space algebra in the center-of-mass and relative coordinate frames for unequal test masses. The aim of Appendix B is to derive the explicit structure of the purity function. Appendix C provides a generalization of our system's potential and its consequences.

II. TWO-PARTICLE SYSTEM: CLASSICAL PICTURE

We begin by considering a pair of nonrelativistic, oppositely charged particles with equal mass m moving on the
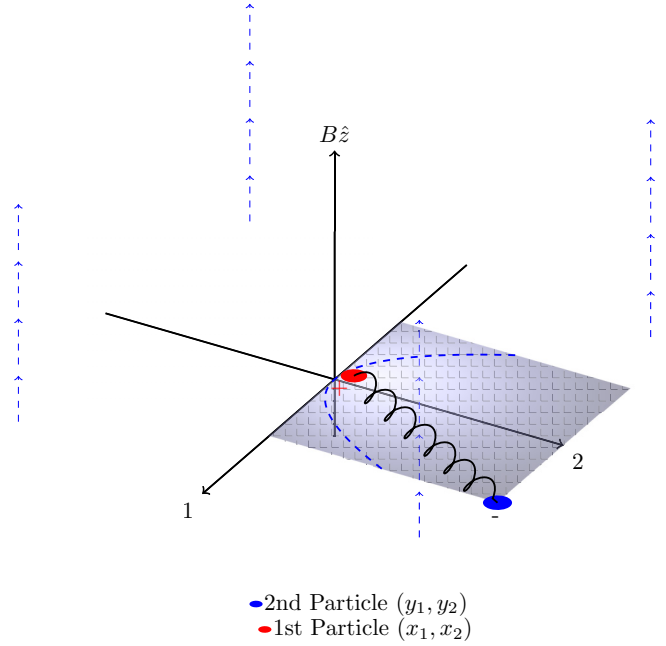

FIG. 1. Magnetic field (blue dashed lines) aligned along the z axis, represented by field lines at different z coordinates. The shaded parabolic potential well along the 1 axis is depicted with a grid pattern, indicating its shape and position. A positively charged particle (red circle, labeled $+$) is located within the well, while a negatively charged particle (blue circle, labeled $-$) is outside the well. These particles are connected by a spring (black wavy line), symbolizing an interaction between them. The blue dashed curve within the shaded region represents the potential profile in the x_1 direction.

plane subjected to a constant magnetic field B along the z axis, ignoring Coulomb and radiation effects (see Fig. 1). In component form, x_i and y_i ($i = 1, 2$) represent the positive- and negative-charge coordinates, respectively. The coordinate z can be suppressed because the dynamics of the system is confined to a plane.

A standard Lagrangian in cgs units is used to define the system as [54–56]

$$L = \frac{1}{2}m(\dot{x}_i^2 + \dot{y}_i^2) + \frac{eB}{2c}\epsilon_{ij}(x_j\dot{x}_i - y_j\dot{y}_i)$$
$$- \frac{K_0}{2}(x_i - y_i)^2 - V(x_1), \quad i, j = 1, 2, \quad (1)$$

where c is the speed of light in a vacuum, ϵ_{ij} is the Levi-Cività symbol, and K_0 is the spring constant corresponding to the harmonic interaction between the two oppositely charged particles. This model is constructed in the spirit of the two-dimensional (2D) excitonic dipole model [57–59], wherein m can be realized by the effective mass of the electron-hole pair in some specific cases where the magnitude of the effective mass of electrons and holes can be considered as approximately the same and the Fermi velocity provides an upper bound for its characteristic velocity in a real physical solid-state system. Note that the first term of the above Lagrangian (1) represents the kinetic term of the charges and the second term represents their interaction with the external magnetic field $\vec{B}$. We use a rotationally symmetric gauge to

define the vector potential $\vec{A}$ satisfying the equation $\vec{\nabla} \times \vec{A} = B\hat{z}$. The third term is the harmonic interaction between the two charges. Finally, the fourth term describes the additional interaction of the positive charge with an impurity in the x_1 direction. The limit of a strong magnetic field B and small mass m such as $\frac{m}{eB} \to 0$ is of interest here, in which the kinetic energy term becomes negligible in the Lagrangian (1) [60]. Thus, we may approximate the dynamics by the effective Lagrangian

$$L_{\text{eff}} = \frac{eB}{2c}\epsilon_{ij}(x_j\dot{x}_i - y_j\dot{y}_i) - V_0(x_i, y_i), \qquad (2)$$

where $V_0(x_i, y_i) = \frac{K_0}{2}(x_i - y_i)^2 + V(x_1)$.

The Lagrangian equations of motion of the coordinates of the positively and negatively charged particles are given by

$$\dot{x}_i = \frac{c}{eB}\epsilon_{ij}\frac{\partial V_0}{\partial x_j}, \quad \dot{y}_i = -\frac{c}{eB}\epsilon_{ij}\frac{\partial V_0}{\partial y_j}. \qquad (3)$$

Since our effective Lagrangian (2) is in first-order form, the effective Hamiltonian of the model is given by

$$H_{\text{eff}} = V_0(x_i, y_i). \qquad (4)$$

In order to show the equivalence between the Lagrangian and Hamiltonian formalism [61,62], we consider Hamilton's equations of motion

$$\dot{x}_i = \{x_i, H_{\text{eff}}\}_{\text{SB}} = \{x_i, V_0(x_i, y_i)\}_{\text{SB}}, \qquad (5)$$

$$\dot{y}_i = \{y_i, H_{\text{eff}}\}_{\text{SB}} = \{y_i, V_0(x_i, y_i)\}_{\text{SB}}, \qquad (6)$$

where $\{\,,\,\}_{\text{SB}}$ denotes the classical symplectic brackets. The nontrivial symplectic structure can be readily obtained by comparing the Lagrangian equations of motion (3) with the form of Hamilton's equations of motion (5) and (6), yielding the following brackets:

$$\{x_i, x_j\}_{\text{SB}} = \frac{c}{eB}\epsilon_{ij}, \quad \{y_i, y_j\}_{\text{SB}} = -\frac{c}{eB}\epsilon_{ij}, \quad \{y_i, x_j\}_{\text{SB}} = 0. \qquad (7)$$

The canonical spatial translation generators for individual charged particles are given by

$$P_{x_i} = \frac{eB}{c}\epsilon_{ij}x_j, \quad P_{y_i} = -\frac{eB}{c}\epsilon_{ij}y_j. \qquad (8)$$

Using the above expressions and the nontrivial symplectic structures between the position coordinates (7), it can be checked that the momentum coordinates also satisfy a nontrivial symplectic bracket, given by

$$\{P_{x_i}, P_{x_j}\}_{\text{SB}} = \frac{eB}{c}\epsilon_{ij}, \quad \{P_{y_i}, P_{y_j}\}_{\text{SB}} = -\frac{eB}{c}\epsilon_{ij},$$
$$\{x_i, P_{x_j}\}_{\text{SB}} = \{y_i, P_{y_j}\}_{\text{SB}} = \delta_{ij}. \qquad (9)$$

In our model, it may be noted that we have considered a sufficiently strong magnetic field such that the kinetic energy of the charged particles is not dominant compared to the magnetic term. In the ultrastrong magnetic regime, the kinetic energy becomes negligible and its effects are entirely suppressed [38,63]. The energy scale associated with a strong magnetic field corresponds to the shortest distance, and one may think that the motion of the charged particle at this

length scale may be treated relativistically. However, the magnetic quantum length scale is $l_B = \sqrt{\frac{\hbar c}{eB}} \approx 10^{-8}$ m, where the magnetic field B is on the order of approximately 10^3 G. The Compton wavelength is given by $\lambda_c = \frac{h}{m_e^* c}$, where m_e^* is the effective mass of the electron, ranging from 0.01 to 10 times the mass of a free electron m_e. The maximum Compton wavelength $(\lambda_c)_{\text{max}}$ is approximately 10^{-10} m, assuming $m_e^* = 0.01m_e$ [64], which is much smaller compared to l_B. It is well known that relativistic effects become significant when the length scale associated with the particle is comparable to or in the vicinity of the Compton wavelength of the particle (see [65] for further details). Therefore, the relativistic nature of our toy model can be completely neglected and it can be treated as a nonrelativistic model.

III. QUANTUM DYNAMICS

In this section we discuss the quantum theory of our nonrelativistic two-particle model at the strong-magnetic-field limit by elevating the phase-space variables to the level of quantum operators. We obtain the nontrivial or unusual commutation brackets $[\,,\,] = i\hbar\{\,,\,\}_{\text{SB}}$ between the position operators given by

$$[\hat{x}_i, \hat{x}_j] = il_B^2\epsilon_{ij}, \quad [\hat{y}_i, \hat{y}_j] = -il_B^2\epsilon_{ij},$$
$$[\hat{x}_i, \hat{y}_j] = 0, \quad i, j = 1, 2, \qquad (10)$$

with $l_B = \sqrt{\frac{\hbar c}{eB}}$ known as the magnetic quantum length scale. Likewise, the other nontrivial phase-space noncommutative algebras are given as

$$[\hat{P}_{x_i}, \hat{P}_{x_j}] = i\frac{\hbar^2}{l_B^2}\epsilon_{ij}, \quad [\hat{P}_{y_i}, \hat{P}_{y_j}] = -i\frac{\hbar^2}{l_B^2}\epsilon_{ij}, \qquad (11)$$

$$[\hat{x}_i, \hat{P}_{x_j}] = [\hat{y}_i, \hat{P}_{y_j}] = i\hbar\delta_{ij}. \qquad (12)$$

It may be observed that, in this case, neither the coordinates nor the momentum operators commute [66]. However, the operators

$$\hat{P}_i = \hat{P}_{x_i} + \hat{P}_{y_i} = \frac{eB}{c}\epsilon_{ij}(\hat{x}_j - \hat{y}_j) \qquad (13)$$

can act as proper (commutative) translation generators so that they satisfy the commutation relations

$$[\hat{x}_i, \hat{x}_j] = il_B^2\epsilon_{ij}, \quad [\hat{P}_i, \hat{P}_j] = 0, \quad [\hat{x}_i, \hat{P}_j] = i\hbar\delta_{ij}, \qquad (14)$$

which represent a noncommutative Heisenberg algebra (NCHA) in two dimensions. In this instance, the operator-valued Hamiltonian of the effective system is given by

$$\hat{H}_{\text{eff}} = \frac{K_0}{2}(\hat{x}_i - \hat{y}_i)^2 + V(\hat{x}_1). \qquad (15)$$

A more conventional setting of this Hamiltonian in terms of the commutative translation generator $\hat{P}_i$ is

$$\hat{H}_{\text{eff}} = \frac{1}{2m_B}\hat{P}_i^2 + V(\hat{x}_1), \quad i = 1, 2, \qquad (16)$$

where $m_B = \frac{e^2B^2}{c^2K_0}$ is the effective mass of the reduced two-particle system. It turns out to be instructive to introduce the

pair of canonical variables

$$\hat{R}_i = \frac{\hat{x}_i + \hat{y}_i}{2}, \quad \hat{P}_i = \frac{eB}{c}\epsilon_{ij}(\hat{x}_j - \hat{y}_j), \quad i, j = 1, 2, \quad (17)$$

where $\hat{R}_i$ is the center-of-mass coordinate and $\hat{P}_i$ is the corresponding canonical momentum of our two-particle system. They satisfy the usual Heisenberg commutation relations as

$$[\hat{R}_i, \hat{R}_j] = 0, \quad [\hat{P}_i, \hat{P}_j] = 0, \quad [\hat{R}_i, \hat{P}_j] = i\hbar\delta_{ij}. \quad (18)$$

However, it is worth noting that the center-of-mass position coordinates may also satisfy NCHA if the two particles are assumed to have different masses (for further details, see Appendix A). Even if the two particles have the same mass, but their position coordinates satisfy NCHA with different noncommutativity parameters, in that case also the center-of-mass position coordinates can give rise to a noncommutative algebra.

Note further that since the dynamics of the composite system is realized in terms of the coordinates of the positively charged particle, the information of the negatively charged particle is completely suppressed in Eqs. (14) and (16), but it is incorporated into the expression of commuting momentum operators. The extended Heisenberg algebra of the type considered in Eq. (14) has the important property that it is realizable in terms of commutative usual phase-space variables (17) as

$$\hat{x}_1 = \text{ad}_{\hat{U}}(\hat{R}_1), \quad \hat{P}_1 = \text{ad}_{\hat{U}}(\hat{P}_1), \quad (19)$$

$$\hat{x}_2 = \text{ad}_{\hat{U}^\dagger}(\hat{R}_2), \quad \hat{P}_2 = \text{ad}_{\hat{U}^\dagger}(\hat{P}_2), \quad (20)$$

where we have made use of the fact of adjoint action $\text{ad}_{\hat{U}}(\hat{A}) = \hat{U}\hat{A}\hat{U}^\dagger$ with a quasiunitary operator $\hat{U}$,

$$\hat{U} = \exp\left[\left(-\frac{il_B^2}{2\hbar^2}\right)\hat{P}_1\hat{P}_2\right], \quad (21)$$

as it does not act unitarily on the entirely noncommutative phase space.

We can observe from Eqs. (19) and (20) that the noncommutative phase-space commutation algebra (14) can be simulated in terms of commutative phase-space variables (canonical variables), i.e., the center-of mass coordinates, as

$$\hat{x}_i = \hat{R}_i - \frac{c}{2eB}\epsilon_{ij}\hat{P}_j, \quad i, j = 1, 2. \quad (22)$$

It may be noted that this transformation is not canonical because it changes the commutation brackets. This transformation has occasionally been called a Darboux map [67] or Bopp's shift [68], which is of relevance in the Bohmian interpretation of noncommutative quantum mechanics [69]. Furthermore, this transformation with an explicit dependence on the deformation parameter allows us to convert the Hamiltonian in noncommutative space into a modified Hamiltonian in commutative equivalent space. It follows that if we are able to solve the spectrum of the system Hamiltonian in commutative equivalent space, we can also obtain the spectrum of the system in primitive noncommutative space, though the states in both situations are not the same. We will discuss how the aforementioned maps aid in the extraction of nonclassical cat states in the next section.

IV. PREPARATION OF SCHRÖDINGER CAT STATES

Using the formalism presented in the preceding section, we are now in a position to investigate the main goal of this work, viz., how we might naturally prepare Schrödinger's cat states. To do so, we first consider a particular Hamiltonian with a harmonic-oscillator potential in the $\hat{x}_1$ direction, given by

$$\hat{H}_{\text{eff}} \rightarrow \hat{H}_{\text{NC}} = \frac{\hat{P}_1^2}{2m_B} + \frac{\hat{P}_2^2}{2m_B} + V(\hat{x}_1), \quad (23)$$

where $V(\hat{x}_1) = \frac{1}{2}K\hat{x}_1^2$ and $m_B = \frac{e^2B^2}{c^2K_0}$. The corresponding time-dependent Schrödinger equation is

$$i\hbar\frac{\partial}{\partial t}|\psi(t)\rangle_{\text{NC}} = \hat{H}_{\text{NC}}|\psi(t)\rangle_{\text{NC}}. \quad (24)$$

Furthermore, because of the noncommutativity of this theory, it is impossible to construct simultaneous eigenstates with noncommutative coordinates, which makes it difficult to define a local probability density for the wave function that corresponds to a particular state $|\psi(t)\rangle_{\text{NC}}$ [70]. However, this issue can be bypassed by using the interpretation mentioned in [70] or by using the coherent states formulation of noncommutative quantum mechanics with the help of the Voros product [71].

In our present case, it can be easily observed that the system Hamiltonian mentioned above can be rewritten as

$$\hat{H}_{\text{NC}} = \hat{U}\hat{H}_{\text{c.m.}}\hat{U}^\dagger, \quad (25)$$

with

$$\hat{H}_{\text{c.m.}} = \frac{\hat{P}_1^2}{2m_B} + \frac{\hat{P}_2^2}{2m_B} + V(\hat{R}_1), \quad (26)$$

where we have used the fact that $V(\hat{x}_1) = V(\hat{U}\hat{R}_1\hat{U}^\dagger) = \hat{U}V(\hat{R}_1)\hat{U}^\dagger$. Here $\hat{H}_{\text{c.m.}}$ is the unitarily equivalent form of the system Hamiltonian expressed in terms of the center-of-mass (c.m.) coordinates, whereas the $\hat{H}_{\text{NC}}$ represents the system Hamiltonian written in terms of the positively charged particle coordinates. We can readily recognize that $V(\hat{R}_1) = \frac{1}{2}K\hat{R}_1^2$, where K is the spring constant of the impurity interaction faced by the positive charge in the $\hat{x}_1$ direction only. Accordingly, the Schrödinger equation (24) transforms as

$$i\hbar\frac{\partial}{\partial t}|\psi(t)\rangle_{\text{c.m.}} = \hat{H}_{\text{c.m.}}|\psi(t)\rangle_{\text{c.m.}}, \quad (27)$$

where $|\psi(t)\rangle_{\text{c.m.}} = \hat{U}^\dagger|\psi(t)\rangle_{\text{NC}}$.

To describe the natural generation of entangled cat states, we consider the appropriate eigenstates of the unitarily equivalent Hamiltonian $\hat{H}_{\text{c.m.}}$, now presented as

$$|\psi_0\rangle_{\text{c.m.}} = |0\rangle \otimes (d_+|+k_2\rangle + d_-|-k_2\rangle), \quad (28)$$

where $|d_+|^2$ and $|d_-|^2$ denote the probability of finding the free particle with nonzero momentum in $|+k_2\rangle$ and $|-k_2\rangle$ states, respectively, and $|0\rangle$ represents the ground state of the 1D harmonic-oscillator system with $\hat{a}_1$ and $\hat{a}_1^\dagger$ representing the corresponding annihilation and creation operators, respectively, satisfying the algebra

$$[\hat{a}_1, \hat{a}_1^\dagger] = \mathbb{I}, \quad \hat{a}_1 = \frac{m_B\omega_B\hat{R}_1 + i\hat{P}_1}{\sqrt{2m_B\omega_B\hbar}}, \quad \hat{a}_1|0\rangle = 0, \quad (29)$$

where $\omega_B = \sqrt{\frac{K}{m_B}}$, and $|\pm k_2\rangle$ corresponds to the right- and left-moving free particle's momentum states, respectively, which satisfy

$$\hat{P}_2|\pm k_2\rangle = \pm P_2|\pm k_2\rangle, \quad P_2 = \hbar k_2. \tag{30}$$

The state vector corresponding to the noncommutative phase space (or in terms of the positively charged particle coordinates) is given by

$$|\psi_0\rangle_{\text{NC}} = \hat{U}|\psi_0\rangle_{\text{c.m.}}, \tag{31}$$

where $|\psi_0\rangle_{\text{NC}}$ can be expressed as

$$|\psi_0\rangle_{\text{NC}} = \left\{ \exp\left[\left(-\frac{il_B^2}{2\hbar^2} \right)\hat{P}_1 \otimes \hat{P}_2 \right] \right\}[|0\rangle \otimes (d_+|+k_2\rangle + d_-|-k_2\rangle)], \tag{32}$$

which leads to

$$|\psi_0\rangle_{\text{NC}} = d_+ \left\{ \left[\exp\left(-\frac{il_B^2 k_2}{2\hbar}\hat{P}_1 \right) \right]|0\rangle \right\} \otimes |+k_2\rangle + d_- \left\{ \left[\exp\left(\frac{il_B^2 k_2}{2\hbar}\hat{P}_1 \right) \right]|0\rangle \right\} \otimes |-k_2\rangle. \tag{33}$$

On substituting $l_B^2 = \frac{\hbar c}{eB}$ in this equation, we arrive at

$$|\psi_0\rangle_{\text{NC}} = d_+ \left(\left\{ \exp\left[\left(-i\frac{ck_2}{2eB} \right)\hat{P}_1 \right] \right\}|0\rangle \right) \otimes |+k_2\rangle + d_- \left(\left\{ \exp\left[\left(i\frac{ck_2}{2eB} \right)\hat{P}_1 \right] \right\}|0\rangle \right) \otimes |-k_2\rangle. \tag{34}$$

Now, for a harmonic-oscillator potential, the momentum operator $\hat{P}_1$ can be written as

$$\hat{P}_1 = i\sqrt{\frac{m_B \omega_B \hbar}{2}}(\hat{a}_1^\dagger - \hat{a}_1). \tag{35}$$

Putting this expression in Eq. (33), we obtain

$$|\psi_0\rangle_{\text{NC}} = d_+ \left(\left\{ \exp\left[\left(\frac{ck_2}{2eB} \right)\sqrt{\frac{m_B \omega_B \hbar}{2}}(\hat{a}_1^\dagger - \hat{a}_1) \right] \right\}|0\rangle \right) \otimes |+k_2\rangle$$
$$+ d_- \left(\left\{ \exp\left[\left(-\frac{ck_2}{2eB} \right)\sqrt{\frac{m_B \omega_B \hbar}{2}}(\hat{a}_1^\dagger - \hat{a}_1) \right] \right\}|0\rangle \right) \otimes |-k_2\rangle. \tag{36}$$

It follows that the above state vector (36) may also be written in the form of a superposition of single-component coherent states as

$$|\psi_0\rangle_{\text{NC}} = d_+|+\alpha\rangle \otimes |+k_2\rangle + d_-|-\alpha\rangle \otimes |-k_2\rangle, \tag{37}$$

wherein $|\pm\alpha\rangle = e^{\pm\alpha(\hat{a}_1^\dagger - \hat{a}_1)}|0\rangle$, with $\alpha = \frac{ck_2}{2eB}\sqrt{\frac{m_B \omega_B \hbar}{2}}$ real-valued coherent states (or a displacement of the vacuum) that belong to the subset of the overcomplete space of usual complex parameter-valued coherent states [72].

Here it may be worthwhile to mention a property of the coherent state $|\pm\alpha\rangle$: The dimensionless parameter α may be rewritten as

$$\alpha = \frac{1}{2}P_2\left(\frac{K}{K_0} \right)^{1/4}\sqrt{\frac{c}{2eB\hbar}} = \xi k_2 l_B, \tag{38}$$

with $\xi = \frac{1}{2}(\frac{K}{4K_0})^{1/4}$. A coherent state $|\alpha\rangle$ can have an arbitrarily large amplitude and hence the energy of a macroscopic harmonic oscillator [73] can be approximated by the energy of a one-dimensional quantum-mechanical harmonic oscillator by suitably choosing $|\alpha|$ to be arbitrarily large. For large enough $|\alpha|$ values, $|+\alpha\rangle$ and $|-\alpha\rangle$ correspond to macroscopically distinguishable states and may be labeled as $+$ (alive) and $-$ (dead) [74,75]. In this sense, we can regard the above state (37) as an entangled SCS, holding $|\alpha|\sqrt{h}$ fixed with

finite value in the classical limit [76,77]. Accordingly, one may consider $|\pm\alpha\rangle$ to be classical-like states, but their coherent superposition is endowed with nonclassical properties. A similar type of Schrödinger cat state has been explored in the context of Rydberg atomic systems using pulsed signals [78], where the coherent (classical) states are coupled with the internal spin states of the atom. However, in our present case, the coherent states are coupled with the left- and right-moving free-particle states.

In the primitive noncommutative phase space, we may rewrite the state vectors (36) concisely as

$$|\psi_0\rangle_{\text{NC}} \to |\boxtimes\rangle = \mathcal{N}[|+\alpha; +k_2\rangle + e^{i\phi}|-\alpha; -k_2\rangle],$$
$$|\pm\alpha; \pm k_2\rangle = |\pm\alpha\rangle \otimes |\pm k_2\rangle, \tag{39}$$

with an arbitrary phase factor ϕ and normalization constant $\mathcal{N}$. For the aforementioned reason, the states $|\pm\alpha\rangle$ may be considered to be macroscopiclike states with the same amplitude but opposite in phase. (In the present case, the $|\alpha|$ parameter is not arbitrary, but is defined in terms of the spring constants, magnetic field, and electric charge.) However, their superposition (39) has several nonclassical characteristics [79]. In particular, for the relative phase factor $e^{i\phi} = \pm 1$, we get even and odd cat states that have been well studied in the literature [4,5]. Moreover, it is evident from (39) that the

coherent states and the free-particle states are entangled: When the coherent state parameter has a positive sign, the free particle state is right moving. On the other hand, the free-particle state is left moving when the coherent state parameter has a negative sign. Therefore, $|\psi_0\rangle_{NC}$ is an entangled Schrödinger cat state containing the coherent superposition [80,81] of two states that are diametrically opposite to one another.

It may be emphasized that in our model, the free-particle-like nature in the $\hat{x}_2$ direction plays a pivotal role in generating left-right superposition states. These states can entangle with coherent states to form catlike states. A specific superposition of free-particle states can also form a localized free-particle state (wave packet), exhibiting multicomponent cat states. In this regard, it is important to emphasize that the free-particle nature in the $\hat{x}_2$ direction of our model is only an effective description of the system under very-strong-magnetic-field conditions. In solid-state physics, the concept of free particles often serves as a starting point to describe more complex systems. Specifically, in semiconductors, the effective-mass approximation allows us to treat electrons in the conduction band and holes in the valence band as free particles. Near the bottom of the conduction band or the top of the valence band, the energy-momentum relationship can be approximated by a parabolic dispersion relation, similar to that of a free particle. These are often referred to as quasifree particles, simplifying the analysis of electronic and optical properties.

Since a momentum eigenstate is an idealization [82], we consider a more realistic scenario in which the system's motion in the commutative phase space is localized within a specific length scale σ in the $\hat{R}_2$ direction. In this case, we generalize the notion of free-particle states to a propagating Gaussian state given by

$$|\psi_G\rangle = \sqrt{\frac{\sigma}{\sqrt{\pi}}} \int_{-\infty}^{+\infty} e^{-(\sigma^2/2)(k_2-k_0)^2}|k_2\rangle dk_2, \quad (40)$$

where σ is the width and k_0 is the peak momentum of the wave packet. Now, following the prescription of (28), we can write the composite state of the particle, when the dynamics of the system is realized in terms of the center-of-mass coordinates, as

$$|\psi_0\rangle_{c.m.} = |0\rangle \otimes |\psi_G\rangle. \quad (41)$$

Accordingly, we can generalize the notion of a two-component cat state (39) to

$$|\boxtimes\rangle = \hat{U}|\psi\rangle_{c.m.} = \sqrt{\frac{\sigma}{\sqrt{\pi}}} \int_{-\infty}^{+\infty} |\alpha(k_2)\rangle$$
$$\otimes |k_2\rangle e^{-(\sigma^2/2)(k_2-k_0)^2} dk_2, \quad (42)$$

which describes a multicomponent entangled Schrödinger cat state [83] where each component is specified through the momentum eigenvalues. Such a state is highly nonclassical, which can be verified through the corresponding Wigner function [83]. Thus, in the presence of a strong-magnetic-field background, one may successfully prepare a Schrödinger cat state utilizing a nonrelativistic electric dipole model, where noncommutativity plays an important role. It may be reiterated here that we explore the system in terms of the positively charged particle coordinates.

Note that we specifically consider the impurity potential attached to the positively charged particle to depend solely on one direction, $\hat{x}_1$. This is crucial for achieving our desired outcome. Introducing a similar (harmonic-oscillator) type of potential in the $\hat{x}_2$ direction would bring the noncommutative nature of the two components, $[\hat{x}_1, \hat{x}_2] \neq 0$, into effect. Transforming the ground state $|\Psi_g\rangle_{c.m.}$ to $\hat{U}|\Psi_g\rangle_{c.m.}$ with the unitary operator $\hat{U}$ would result in a superposition of displaced number states rather than coherent states. This transformation disrupts the coherent superposition of states necessary for realizing catlike states. Therefore, we consider the potential as a function of only $\hat{x}_1$ to naturally demonstrate the emergence of catlike states. Similarly, if we attach the potential along $\hat{y}_1$ with the negatively charged particle, the potential term affects the dynamics of the first charged particle in the presence of the potential attached to the positively charged particle in the $\hat{x}_1$ direction. This effectively introduces a coupling between the two modes of the positively charged particles with respect to the center-of-mass frame, resulting in the loss of the coherent superposition of coherent states, thus preventing the formation of catlike states. This indicates that achieving catlike states is possible only for a specific class of potentials, which should be attached to either the positively charged particle or the negatively charged particle in a single direction, rather than applying potentials to both charged particles in both directions. For more details, see Appendix C.

V. COLLAPSE AND REVIVAL OF ENTANGLEMENT OF THE SCS

In this section we begin by investigating the degree of entanglement of the SCS $|\psi\rangle_{NC}$. In order to do so, we first write the corresponding density matrix given by

$$\hat{\rho}_{NC} = \left(\sqrt{\frac{\sigma}{\sqrt{\pi}}}\right)^2 \int_{-\infty}^{+\infty}\int_{-\infty}^{+\infty} [|\alpha(k_2)\rangle_A \langle\alpha(k_2')|]$$
$$\otimes [|k_2\rangle_B \langle k_2'|] e^{(-\sigma^2/2)(k_2-k_0)^2} e^{(-\sigma^2/2)(k_2'-k_0)^2} dk_2 dk_2', \quad (43)$$

where the subscripts A and B denote two distinct subsections of our bipartite system, one of which is associated with coherent states and the other with momentum eigenstates, each of which corresponds to two distinct degrees of freedom in the noncommutative plane. Since $|\psi\rangle_{NC}$ is a composite pure state, the entanglement between the coherent states and free-particle states can be quantified in terms of the von Neumann entropy given by

$$S = -\text{Tr}_A[\hat{\rho}_{red}\ln(\hat{\rho}_{red})], \quad (44)$$

where the reduced density matrix is defined as

$$\hat{\rho}_{red} = \text{Tr}_B(\hat{\rho}_{NC})$$
$$= \frac{\sigma}{\sqrt{\pi}} \int_{-\infty}^{+\infty} [|\alpha(k_2)\rangle_A \langle\alpha(k_2)|] e^{-\sigma^2(k_2-k_0)^2} dk_2, \quad (45)$$

with

$$\text{Tr}(\hat{\rho}_{red}) = \frac{\sigma}{\sqrt{\pi}} \int_{-\infty}^{+\infty} e^{-\sigma^2(k_2-k_0)^2} dk_2 = 1. \quad (46)$$

For the present purpose, it suffices to compute the purity function [84], given by

$$P(\alpha) = \mathrm{Tr}\big(\hat{\rho}_{\mathrm{red}}^2\big) = \sum_n \langle n|\hat{\rho}_{\mathrm{red}}^2|n\rangle = \sum_m \sum_n \langle n|\hat{\rho}_{\mathrm{red}}|m\rangle \langle m|\hat{\rho}_{\mathrm{red}}|n\rangle. \qquad (47)$$

After a little algebra, we obtain

$$\langle n|\hat{\rho}_{\mathrm{red}}|m\rangle = \frac{\sigma}{\sqrt{\xi^2 l_B^2 + \sigma^2}} \frac{1}{\sqrt{n!}\sqrt{m!}} e^{-\sigma^2 k_0^2} \left(\frac{\xi l_B}{2\sigma^2}\right)^{n+m} \frac{\partial^{n+m}}{\partial k_0^{n+m}} e^{\sigma^4 k_0^2/(\xi^2 l_B^2 + \sigma^2)}. \qquad (48)$$

By inserting Eq. (48) into (47) it follows that

$$P(\xi_0; l_B) = \left(\frac{1}{1+\xi_0^2}\right) e^{-2\sigma^2 k_0^2} \left[\exp\left(\frac{\sigma^2 k_0^2}{1+\xi_0^2}\right) \exp\left(\frac{\xi_0^2}{2\sigma^2} \overleftarrow{\frac{\partial}{\partial k_0}} \overrightarrow{\frac{\partial}{\partial k_0}}\right) \exp\left(\frac{\sigma^2 k_0^2}{1+\xi_0^2}\right) \right], \qquad (49)$$

where $\xi_0 = \frac{\xi l_B}{\sigma}$ and $\xi = \frac{1}{2}(\frac{K}{4K_0})^{1/4}$ as defined in Eq. (38). The expression (49) can be rewritten (see Appendix B) as

$$P(\xi_0; l_B) = \frac{1}{\sqrt{1+2\xi_0^2}}. \qquad (50)$$

In Fig. 2 we plot the purity function versus the parameter ξ_0. It can be observed that the purity function reduces from unit value (separable or disentangled state) with an increase of the parameter ξ_0, indicating the increment of entanglement in the system for higher values of ξ_0 (or lower values of the width of the wave packet σ). We consider the quantum length scale $l_B = 1.483 \times 10^{-8}$ m and vary the width of the wave packet in the range of $O(10^{-11}–10^{-6})$. Different l_B values displayed in the figure may originate due to the variation of the magnetic length scale with different accessible magnetic fields in the laboratory.

It may be noted that if we just assume $\xi_0 \ll 1$ with $\xi \sim 1$, which implies that $l_B \ll \sigma$, i.e., the width of the Gaussian packet σ is large enough compared to the magnetic quantum length scale such that we can ignore ξ_0, then it leads to the unit value of the purity function or, in other words, the collapse
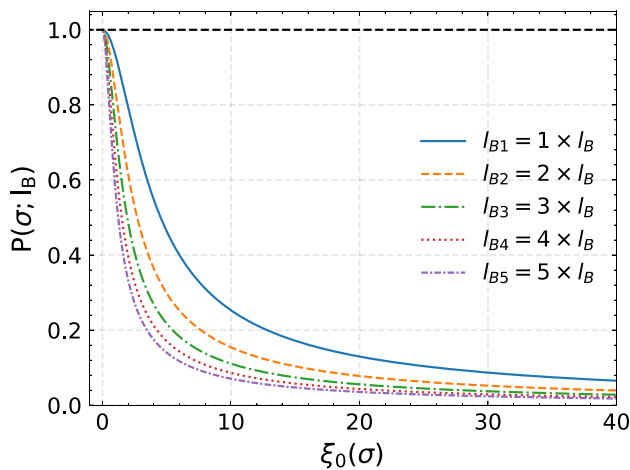
of the entanglement in the state. On the other hand, we can make the states entangled by choosing σ comparable to the magnetic length scale l_B where $P(\xi_0; B)$ becomes less than unity. More interestingly, the revival of the entanglement state can occur if one considers a time-dependent regime. Let us recall from the definition of ξ that it basically depends on the coupling strength K of the impurity interaction.

The dynamic behavior of impurities in materials is known to lead to time-varying spring interaction [85,86]. Such a dynamic nature of the coupling has been studied in the literature in the context of several physical systems such as in optical lattices [87] and extensively in the domain of quantum electronic transport [88–90]. Let us now consider that the spring constant K is a slowly varying periodic function of time due to some external effects, with the time variation given by

$$K \to K(t) = K \cos^4 \omega_d t = K \cos^4 \theta(t), \qquad (51)$$

which clearly indicates $\xi(t) = \frac{1}{2}(\frac{K\cos^4 \omega_d t}{4K_0})^{(1/4)}$ and $\xi_0(t) = \frac{\xi(t) l_B}{\sigma}$. Hence, the purity function gets modified to

$$P(\xi_0; l_B) = \frac{1}{\sqrt{1+2\xi_0^2(t)}}. \qquad (52)$$

Before we proceed further, the following comments are in order. It may be noted that the expression above ensures that the purity function (52) remains real at any arbitrary instant t within the time period. Considering a simple form $K(t) = K \cos^n(\omega_d t)$ with $\xi(t=0) \sim 1$ to highlight the main features, we observe that $\xi_0(t) \sim \cos^{n/4}(\omega_d t)$. The reality condition of the purity function is satisfied only when we limit ourselves to $n/2$ being an even integer. For the purpose of highlighting the main features of the dynamical behavior of entanglement, we choose the smallest integer $n = 4$. The periodic behavior of the purity function gives rise to the phenomenon of collapse and revival of entanglement, as we now show.

It should be noted that even when σ is comparable to the magnetic length scale l_B, disentanglement occurs in specific instances such as $t_d = \frac{\pi}{2\omega_d}, \frac{3\pi}{2\omega_d}, \frac{5\pi}{2\omega_d}, \frac{7\pi}{2\omega_d}, \ldots$ with a separation of the time period $\frac{\pi}{\omega_d}$ between two successive collapses. For the rest of the time interval, the states are entangled. This distinguishing feature is known as the collapse and revival of entanglement in the literature [91]. In Fig. 3 we plot the purity function versus the periodic parameter $\theta(t)$ for several different values of the width of the wave packet σ. It is clearly
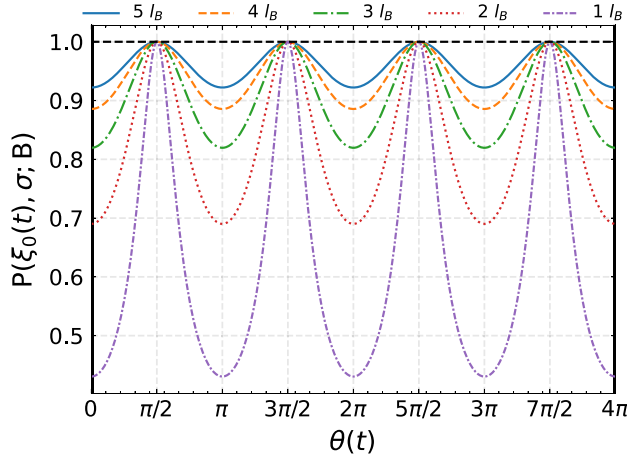

FIG. 2. Purity function plotted against the dimensionless factor ξ_0, which varies inversely with the width of the wave packet σ. Several choices of the quantum length scale are plotted and the direction of the arrow suggests the direction of increment of magnetic fields, which is inversely proportional to the l_B^2.

FIG. 3. Time evolution of the purity function plotted against the parameter $\theta(t)$ for various widths of the wave packets σ.

FIG. 4. Three-dimensional view of a semiconductor layer with *p*-type and *n*-type particles. The axes are labeled x, y, and z. The semiconductor layer is shown with different colors: green for the left face, cyan for the right face, yellow for the bottom face, orange for the top face, and magenta for the front face. The *p*-type particles are shown as red circles on the front layer and the *n*-type particles are shown as blue circles inside the bulk. The electric field is represented by dashed and dotted arrows pointing in the x direction, while the magnetic field is shown by a solid arrow along the z axis. The electric field is given by $\vec{E} = f(\cos \omega_d t)e^{-\alpha_0 x}\vec{E}_0$ and the magnetic field is denoted by $\vec{B}$.

seen that the magnitude of entanglement revival increases more for narrower wave packets.

Here it needs to be mentioned that in order to observe entanglement revival of the states, we are required to choose σ of an order comparable to that of the magnetic length scale l_B or less, as $-1 \leqslant \cos \omega_d t \leqslant +1$. On the other hand, if we choose σ to be much larger than l_B, then the additional term in the denominator of Eq. (52) can be completely negligible, which will take us back again to the situation of the entanglement collapse, viz., $P(\xi_0; B) \sim 1$. Instances of the phenomenon of entanglement collapse and revival have been pointed out earlier in the literature predominantly in the context of the Jaynes-Cummings model for optical systems [53,91]. Here we furnish a striking example of entanglement collapse and revival in the context of an excitonic dipole in a condensed-matter system.

To illustrate the collapse and revival of entanglement in cat states with moving free-particle states, we use a time-dependent spring constant $K(t)$ within our dipole system. The effective masses of electrons and holes, denoted by m, are taken to be of the same order of magnitude, which allows the c.m. coordinates to be treated as commutative with respect to the positively charged particle coordinates [92]. Though the effective masses of electrons and holes generally differ due to the unequal curvature of the valence and conduction bands, it is possible for them to be approximately equal if there exists electron-hole symmetry manifested by the valence-band maxima aligning with the conduction-band minima at the same point. The experimental realization of our model may be feasible in systems involving certain specific direct band-gap semiconductors [93–95], where the minimum conduction band for electrons and the maximum valence band for holes are located at the same point of the Brillouin zone. In these materials, the effective masses of electrons and holes can be quite similar in magnitude, typically arising from specific band structures and symmetries.

A possible realization of our model is illustrated in Fig. 4, involving a time-varying electric field $\vec{E} = f(\cos \omega_d t)e^{-\alpha_0 x}\vec{E}_0$ applied along the x axis, perpendicular to the surface layer where the holes are located [96]. In fact, the holes and elec-
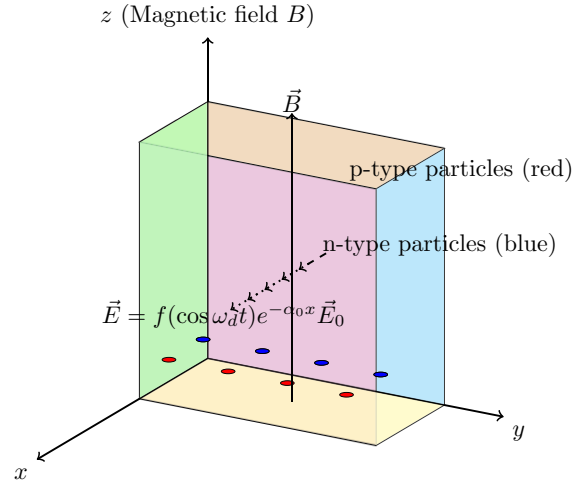
trons, which are confined in the bulk, reside in a plane parallel to the *x*-*y* plane, while a magnetic field is applied along the z axis. This setup is ideal for a heavily doped *p*-type semiconductor, where an accumulation layer of holes is formed near the surface [93,97]. The ac electric field varies slowly (to avoid abrupt changes to the initial state, specifically the ground state of the oscillator trap, which is crucial for demonstrating catlike states), with $e^{-\alpha_0 x}$ ensuring that its primary effect is near the surface. Here, due to the high conductivity of heavily doped *p*-type semiconductors, α_0^{-1} can be approximated by $\alpha_0^{-1} \sim \sqrt{\frac{2}{\sigma \mu \omega_d}}$ (using the approximations of a good conducting medium), where σ, n_h, and μ denote conductivity, hole doping concentration, and permeability of the conducting medium, respectively. For this good conductivity of the *p*-type sample, even low-frequency fields will have a limited penetration depth α_0^{-1}, thus restricting their effect on the bulk material. This limited penetration depth ensures that the field primarily influences surface-localized holes, which aligns with our toy version of the excitonic dipole model. The electric field introduces a time-dependent potential that mimics a time-dependent spring constant $K(t)$ in the Hamiltonian, under suitable attenuation and approximations. By employing $\cos^4(\omega_d t)$, we ensure that the purity function remains real, as discussed after Eq. (52). In fact, any periodic time-dependent function that maintains an oscillatory nature at $t = 0$ (i.e., has a nonzero value at $t = 0$) and satisfies the reality condition of the purity function can serve as the time-dependent spring constant $K(t)$. This allows us to explore phenomena such as the variation of the purity function, the revival and collapse of entanglement, and other related effects.

Before concluding, it may be noted that we have considered a periodic function of time with a slow variation, charac-

terized by a time period $t_d = \frac{2\pi}{\omega_d}$. The degree of adiabaticity, which quantifies the slowness of the process, can be defined as

$$\epsilon = \hbar \frac{|\langle m(t)| \frac{\partial \hat{H}(t)}{\partial t} |n(t)\rangle|}{(E_m - E_n)^2} \sim \frac{\omega_d}{\omega_{mn}}, \qquad (53)$$

where the transitional angular frequency $\omega_{mn} = \frac{E_m - E_n}{\hbar}$ is introduced. Here $\epsilon \ll 1$ signifies that the variation of the Hamiltonian (in terms of matrix elements) over the timescale $\frac{2\pi}{\omega_{nm}}$ is small compared to the energy separation $E_m - E_n$. The adiabatic approximation is valid when this condition is satisfied, serving as a measure of the slowness required for its applicability [98]. The dynamical periodic behavior of the purity function is a natural consequence of a harmonic-oscillator system with a periodically time-varying spring constant in an adiabatic process. In this context, the system can adjust or adopt itself to stay in its initial eigenstates, preserving the real forms of the purity function. Though the adiabatic approach has been invoked here to simplify the technical complexities and extract the essential features of the dynamic nature of entanglement, nonadiabatic time variation may also lead to collapse and revival behavior [99].

VI. CONCLUSION

To summarize, in this work we have considered a composite two-particle planar dipole system in the presence of a strong constant and uniform magnetic field, in which two oppositely charged particles interact via harmonic interaction, in addition to an impurity interaction experienced by the positively charged particle. Our system may be regarded as a toy version of excitonic dipole models that can be realized in some specific direct band-gap semiconductors [93–95] having the conduction-band minimum for electrons and the valence-band maximum for holes both located at the same point of the Brillouin zone, where the effective mass of electrons and holes can be quite similar in magnitude. This typically arises due to specific band structures and symmetries of materials. The additional interaction could arise from intrinsic features such as defects or impurities, as well as from external influences like an external electric field or strain in the material [100].

In our analysis, we first addressed the classical picture in the context of our system's Lagrangian formulation, which is the most natural in a strong-magnetic-field limit. Using symplectic analysis of this first-order Lagrangian, we specified the canonical or Weyl-Moyal-type deformed noncommutative classical phase space to be an intrinsic part of our model. Next we explored the quantum-mechanical description of our model by elevating all the phase-space variables to the level of Hermitian operators. The spatial and momentum sectors of individual charged particles obey a noncommutative deformed algebra. Here the noncommutativity emerges as a natural consequence of placing two oppositely charged particles in a strong constant background magnetic field. The square of the magnetic length scale acts as the effective noncommutative parameter.

We have presented a physical interpretation of the mapping from the deformed phase space to the usual commutative phase space. The noncommutative phase space represents the system Hamiltonian written in terms of the positively charged particle coordinates, while the standard quantum-mechanical phase space is more suitable for describing our system in terms of the composite system's center-of mass coordinates. The dynamics can therefore be analyzed in terms of noncommuting variables or, alternatively, using phase-space transformations, in terms of commuting variables. In the literature, noncommutativity has been often introduced by hand for a single point particle, thus ruling out any physicality of commutative phase-space variables in such cases. However, in the present case, noncommutativity emerges naturally, thereby giving a physical meaning to the commutative phase-space variables. Determining the Hamiltonian's ground state in the commutative phase space allows us to express the quantum state in the noncommutative phase space as a superposition of two diametrically opposite coherent states, entangled with momentum eigenstates. This reveals the emergence of entangled and two-component states as well as multicomponent Schrödinger cat states in our system.

Furthermore, we have estimated the magnitude of entanglement in the system of multicomponent entangled cat states. By utilizing the purity function, we demonstrated that the effective noncommutative parameter l_B^2 is responsible for the entanglement. We showed that when the width of the Gaussian wave packet σ significantly exceeds the minimal length scale l_B, the entangled cat states undergo collapse. Conversely, when σ is comparable to the nonzero magnetic length scale l_B, the entanglement can be observed. Moreover, we showed that if the time-dependent impurity potential is chosen, entanglement revival and collapse occurs periodically. So notably, within the same formalism, we observed the phenomenon of collapse and revival of entanglement in the noncommutative plane in the time-dependent regime with a suitable choice of the σ parameter for the revival case, while the collapse is completely controlled by the nodes of the periodic function involved in the impurity interaction.

Our study explores the natural emergence of Schrödinger cat states in excitonic models, where these states can be conceptualized as qubits [101]. Specifically, the states are represented as superpositions $|+\alpha(k_2)\rangle \otimes |+k_2\rangle \equiv |1\rangle_{k_2}$ and $|-\alpha(k_2)\rangle \otimes |-k_2\rangle \equiv |0\rangle_{k_2}$, where the momentum eigenstates are distinct and isolated, i.e., having zero overlap between $|+k_2\rangle$ and $|-k_2\rangle$. Our approach indicates that multiple components of cat states, which represent superpositions of large qubit collections with fixed momentum eigenvalues, could be used to encode qubits for constructing extensive quantum registers [102]. Many-body effects in excitonic Bose-Einstein condensates can lead to Schrödinger cat states, potentially resulting in new phases of matter at critical temperatures. Additionally, our system has potential applications in quantum error correction by encoding each logical qubit using multimode cat states [18,19]. Experimentation of our model proposing the generation of excitonic cat states can pave a new path for studying the emerging field of optoelectronics exploring fundamental physics of quantum entanglement.

Finally, it may be noted that spin-orbit interactions in solid-state systems introduce electronic band curvature, leading to the emergence of Berry curvature in momentum space. Such Berry curvature modifies the usual phase-space symplectic structure of Bloch electrons [103,104]. In light of noncommutative quantum mechanics, our present analysis can be extended to include investigations on the possible emergence

of Schrödinger cat states in solid-state systems involving the 2D excitonic Coulomb problem with the Berry curvature of the electron's and the hole's Bloch states [57,105,106]. This extension opens a gateway to a new frontier, promising fresh insights and potentially paving the way for the experimental exploration of the macroscopic quantum state of excitons [102].

APPENDIX A

Here we present a manifestation of the noncommutativity of the center-of mass coordinates arising in the case of two oppositely charged particles with different masses m_+ and m_- representing the masses of positively and negatively charged particles, respectively. The corresponding c.m. coordinates of the above-discussed system are

$$
\hat{R}_i = \frac{m_+ \hat{x}_i + m_- \hat{y}_i}{m_+ + m_-},
$$
$$
\hat{P}_i = \hat{P}_{x_i} + \hat{P}_{y_i} = \frac{eB}{c}\epsilon_{ij}(\hat{x}_j - \hat{y}_j), \quad i, j = 1, 2. \quad \text{(A1)}
$$

Now, utilizing the results obtained from Eq. (10), the commutation brackets between the c.m. coordinates can be obtained in the form

$$
[\hat{R}_i, \hat{R}_j] = \frac{m_+^2 - m_-^2}{(m_+ + m_-)^2} i l_B^2 \epsilon_{ij}, \quad i, j = 1, 2, \quad \text{(A2)}
$$

clearly indicating the noncommutativity between the c.m. position coordinates with $\theta = \frac{m_+^2 - m_-^2}{(m_+ + m_-)^2} i l_B^2 \epsilon_{ij}$ being the effective noncommutativity parameter. However, it is straightforward to check that the other two commutation brackets remain preserved:

$$
[\hat{P}_i, \hat{P}_j] = 0, \quad [\hat{R}_i, \hat{R}_j] = i\hbar\delta_{ij}. \quad \text{(A3)}
$$

It may be noted that the order of magnitude of the noncommutativity between the c.m. position coordinates is much lower compared to that of the position coordinates of the individual constituent particles. This is simply because l_B^2 itself is very small due to the strong-magnetic-field limit; the presence of the additional mass factor reduces the whole effective noncommutativity parameter θ to a much smaller value.

Now let us introduce the relative coordinate system

$$
\hat{r}_i = \hat{y}_i - \hat{x}_i, \quad \hat{\bar{P}}_i = \frac{m_+}{m_+ + m_-}\hat{P}_{y_i} - \frac{m_-}{m_+ + m_-}\hat{P}_{x_i}, \quad i = 1, 2. \quad \text{(A4)}
$$

The commutation relations satisfied by the relative coordinates are given by

$$
[\hat{r}_i, \hat{r}_j] = 0, \quad [\hat{\bar{P}}_i, \hat{\bar{P}}_j] = \frac{m_-^2 - m_+^2}{(m_+ + m_-)^2} i \frac{\hbar^2}{l_B^2}\epsilon_{ij},
$$
$$
[\hat{r}_i, \hat{\bar{P}}_j] = i\hbar\delta_{ij}, \quad i, j = 1, 2. \quad \text{(A5)}
$$

It is evident that the relative position coordinates commute as we have considered two oppositely charged particles in a noncommutative space (it has been shown earlier [107] that the noncommutativity of a charged particle differs from its antiparticle and also from any other particle of opposite charge by the sign). On the other hand, the coordinates of relative momenta give rise to a nontrivial commutation algebra with a reduced order of magnitude from that of the individual constituent particle's momentum coordinates.

It may be further noted that the position coordinates of the center-of-mass and the position coordinates of the relative motion are not independent; rather they obey the relation given by

$$
[\hat{R}_i, \hat{r}_j] = -i l_B^2 \epsilon_{ij}, \quad i, j = 1, 2. \quad \text{(A6)}
$$

So clearly there is a connection between the motion of the center of mass and the relative motion of the composite system in the noncommutative space. This helps us reduce the two-body problem completely to a one-body problem for the internal motion in noncommutative space using the c.m. coordinates of the composite system where the information of the negatively charged particle is solely hidden or encoded within the c.m. momenta giving rise to a standard commutative algebra.

APPENDIX B

Here we provide a derivation for the expression of the purity function. We begin with the expression of the reduced density matrix of Eq. (45) and the expression of the coherent state $|\alpha(k_2)\rangle$ and definition of the purity function from Eq. (47),

$$
P(\alpha) = \sum_l \sum_s \langle l|\hat{\rho}_{\text{red}}|s\rangle\langle s|\hat{\rho}_{\text{red}}|l\rangle,
$$
$$
\langle l|\hat{\rho}_{\text{red}}|s\rangle = \frac{\sigma}{\sqrt{\pi}} \int_{-\infty}^{+\infty} \langle l||\alpha(k_2)\rangle\langle\alpha(k_2)||s\rangle e^{-\sigma^2(k_2-k_0)^2} dk_2. \quad \text{(B1)}
$$

The coherent state can be expressed as

$$
|\alpha(k_2)\rangle = e^{-\alpha^2/2}e^{\alpha\hat{a}_1^\dagger}e^{-\alpha\hat{a}_1}|0\rangle = e^{-\alpha^2/2}e^{\alpha\hat{a}_1^\dagger}|0\rangle,
$$
$$
\langle l||\alpha(k_2)\rangle = \langle l|e^{-\alpha^2/2}\sum_{n=0}^\infty \frac{\alpha^n}{\sqrt{n!}}|n\rangle = e^{-\alpha^2/2}\frac{\alpha^l}{\sqrt{l!}}. \quad \text{(B2)}
$$

Similarly, $\langle\alpha(k_2)||s\rangle = e^{-\alpha^2/2}\frac{\alpha^s}{\sqrt{s!}}$. Plugging this into Eq. (A6), we get

$$
\langle l|\hat{\rho}_{\text{red}}|s\rangle = \frac{\sigma}{\sqrt{\pi}} \int_{-\infty}^{+\infty} e^{-\alpha^2}\frac{(\alpha)^{l+s}}{\sqrt{l!}\sqrt{s!}}e^{-\sigma^2(k_2-k_0)^2} dk_2. \quad \text{(B3)}
$$

Now substituting $\alpha(k_2) = \beta k_2$, where $\beta = \xi l_B$, we get

$$\langle l|\hat{\rho}_{\mathrm{red}}|s\rangle = \frac{\sigma}{\sqrt{\pi}} \frac{\beta^{l+s}}{\sqrt{l!}\sqrt{s!}} e^{-\sigma^2 k_0^2} \int_{-\infty}^{+\infty} e^{-(\beta^2+\sigma^2)k_2^2+2\sigma^2 k_0 k_2} k_2^{l+s} dk_2 \tag{B4}$$

$$= \frac{\sigma}{\sqrt{\pi}} \frac{\beta^{l+s}}{\sqrt{l!}\sqrt{s!}} e^{-\sigma^2 k_0^2} \frac{1}{(2\sigma^2)^{l+s}} \frac{\partial^{l+s}}{\partial k_0^{l+s}} \left(\int_{-\infty}^{+\infty} e^{-(\beta^2+\sigma^2)k_2^2+2\sigma^2 k_2 k_0} dk_2 \right) \tag{B5}$$

$$= \frac{\sigma}{\sqrt{\pi}} \frac{\beta^{l+s}}{\sqrt{l!}\sqrt{s!}} e^{-\sigma^2 k_0^2} \frac{1}{(2\sigma^2)^{l+s}} \frac{\partial^{l+s}}{\partial k_0^{l+s}} \left(\sqrt{\frac{\pi}{\beta^2+\sigma^2}} e^{\sigma^4 k_0^2/(\beta^2+\sigma^2)} \right). \tag{B6}$$

Using the above expressions in the purity function, we get

$$P(\alpha) = \frac{\sigma^2}{\beta^2+\sigma^2} e^{(-2\sigma^2 k_0^2)} \sum_l \sum_s \frac{1}{l!s!} \left(\frac{\beta^2}{4\sigma^4} \right)^{l+s} \left(e^{\sigma^4 k_0^2/(\beta^2+\sigma^2)} \frac{\overleftarrow{\partial^{l+s}}}{\partial k_0^{l+s}} \frac{\overrightarrow{\partial^{l+s}}}{\partial k_0^{l+s}} e^{\sigma^4 k_0^2/(\beta^2+\sigma^2)} \right). \tag{B7}$$

Performing the summations, we are led to

$$P(\alpha(k_2)) = \frac{\sigma^2}{\beta^2+\sigma^2} e^{(-2\sigma^2 k_0^2)} \left[e^{\sigma^4 k_0^2/(\beta^2+\sigma^2)} \exp\left(\frac{\beta^2}{2\sigma^4} \frac{\overleftarrow{\partial}}{\partial k_0} \frac{\overrightarrow{\partial}}{\partial k_0} \right) e^{\sigma^4 k_0^2/(\beta^2+\sigma^2)} \right]. \tag{B8}$$

Now, replacing $\xi_0 = \frac{\xi l_B}{\sigma}$, we arrive at

$$P(\xi_0; l_B) = \left(\frac{1}{1+\xi_0^2} \right) e^{-2\sigma^2 k_0^2} \left[e^{\sigma^2 k_0^2/(1+\xi_0^2)} \exp\left(\frac{\xi_0^2}{2\sigma^2} \frac{\overleftarrow{\partial}}{\partial k_0} \frac{\overrightarrow{\partial}}{\partial k_0} \right) e^{\sigma^2 k_0^2/(1+\xi_0^2)} \right]. \tag{B9}$$

Subsequently, we express $e^{\sigma^2 k_0^2/(1+\xi_0^2)} \exp(\frac{\xi_0^2}{2\sigma^2} \frac{\overleftarrow{\partial}}{\partial k_0} \frac{\overrightarrow{\partial}}{\partial k_0}) e^{\sigma^2 k_0^2/(1+\xi_0^2)}$ in a more concise form, where $\frac{\overrightarrow{\partial}}{\partial k_0} f = \frac{\partial f}{\partial k_0}$ and $f \frac{\overleftarrow{\partial}}{\partial k_0} = \frac{\partial f}{\partial k_0}$. For that, let us consider the following integral:

$$\int_{-\infty}^{+\infty} e^{-bs^2+2sk_0} ds = e^{k_0^2/b} \int_{-\infty}^{+\infty} e^{-b(s+k_0/b)^2} ds = e^{k_0^2/b} \sqrt{\frac{\pi}{b}}. \tag{B10}$$

From the expression of $e^{\sigma^2 k_0^2/(1+\xi_0^2)}$ it follows that

$$e^{\sigma^2 k_0^2/(1+\xi_0^2)} = \sqrt{\frac{1+\xi_0^2}{\sigma^2 \pi}} \int_{-\infty}^{+\infty} e^{-[(1+\xi_0^2)/\sigma^2]s^2+2sk_0} ds. \tag{B11}$$

Therefore, using the relation $e^{a\partial/\partial k_0} e^{bk_0} = e^{ab} e^{bk_0}$, we have

$$e^{\sigma^2 k_0^2/(1+\xi_0^2)} \exp\left(\frac{\xi_0^2}{2\sigma^2} \frac{\overleftarrow{\partial}}{\partial k_0} \frac{\overrightarrow{\partial}}{\partial k_0} \right) e^{\sigma^2 k_0^2/(1+\xi_0^2)} = \frac{1+\xi_0^2}{\sigma^2 \pi} \int_{-\infty}^{+\infty} e^{-[(1+\xi_0^2)/\sigma^2]s^2+2sk_0} ds \exp\left(\frac{\xi_0^2}{2\sigma^2} \frac{\overleftarrow{\partial}}{\partial k_0} \frac{\overrightarrow{\partial}}{\partial k_0} \right) \int_{-\infty}^{+\infty} e^{-[(1+\xi_0^2)/\sigma^2]s'^2+2s'k_0} ds'$$

$$= \frac{1+\xi_0^2}{\sigma^2 \pi} \int_{-\infty}^{+\infty} e^{-[(1+\xi_0^2)/\sigma^2]s^2+2sk_0} ds\, e^{2\xi_0^2 ss'/\sigma^2} \int_{-\infty}^{+\infty} e^{-[(1+\xi_0^2)/\sigma^2]s'^2+2s'k_0} ds'$$

$$= \frac{1+\xi_0^2}{\sigma^2 \pi} \int_{-\infty}^{+\infty} e^{-[(1+\xi_0^2)/\sigma^2]s^2+2sk_0} ds \int_{-\infty}^{+\infty} e^{-[(1+\xi_0^2)/\sigma^2]s'^2+2(k_0+\xi_0^2 s/\sigma^2)s'} ds'$$

$$= \sqrt{\frac{1+\xi_0^2}{\sigma^2 \pi}} \int_{-\infty}^{+\infty} e^{-[(1+\xi_0^2)/\sigma^2]s^2+2sk_0} e^{(\sigma^2 k_0+\xi_0^2 s)^2/\sigma^2(1+\xi_0^2)} ds$$

$$= \sqrt{\frac{1+\xi_0^2}{\sigma^2 \pi}} e^{\sigma^2 k_0^2/(1+\xi_0^2)} \int_{-\infty}^{+\infty} e^{-[(1+2\xi_0^2)/\sigma^2(1+\xi_0^2)]s^2+2k_0[(1+2\xi_0^2)/(1+\xi_0^2)]s} ds.$$

After performing some suitable steps, we get the final simplified form

$$e^{\sigma^2 k_0^2/(1+\xi_0^2)} \exp\left(\frac{\xi_0^2}{2\sigma^2} \frac{\overleftarrow{\partial}}{\partial k_0} \frac{\overrightarrow{\partial}}{\partial k_0} \right) e^{\sigma^2 k_0^2/(1+\xi_0^2)} = \frac{1+\xi_0^2}{\sqrt{1+2\xi_0^2}} e^{2\sigma^2 k_0^2}. \tag{B12}$$

Now, after plugging the above result (B12) in Eq. (B9), the expression of the purity function reduces to Eq. (50).

APPENDIX C

Here we discuss how cat-state-like behavior will be affected by generalizing the notion of impurity potential. To see this, we consider the system Hamiltonian in the presence of an impurity potential (a 2D oscillatory potential) attached to a positively charged particle

$$\hat{H}_{NC} = \frac{\hat{P}_1^2}{2m_B} + \frac{\hat{P}_2^2}{2m_B} + V(\hat{x}_1, \hat{x}_2), \qquad (C1)$$

where $V(\hat{x}_1, \hat{x}_2) = \frac{1}{2}K(\hat{x}_1^2 + \hat{x}_2^2)$ and $m_B = \frac{e^2 B^2}{c^2 K_0}$.

It may be noted that $\hat{H}_{NC} = \hat{U}\hat{H}_{c.m.}\hat{U}^\dagger$, where

$$\hat{H}_{c.m.} = \frac{\hat{P}_1^2}{2m_B} + \frac{\hat{P}_2^2}{2m_B} + \frac{1}{2}K\hat{R}_1^2 + \frac{1}{2}K\left(\hat{R}_2 + \frac{c}{eB}\hat{P}_1\right)^2. \quad (C2)$$

Here $\hat{H}_{c.m.}$ indicates that the two modes are no longer independent, as the system Hamiltonian still retains its noncommutative effect through the explicit coupling between $\hat{R}_2$ and $\hat{P}_1$ when realized in terms of center-of-mass phase-space variables. However, this system can be diagonalized by a suitable phase-space transformation [108]. An important point is whether we can still achieve catlike states. We can consider the specific states of $\hat{H}_{c.m.}$, such as the ground state $|\Psi_g\rangle_{c.m.}$, which satisfies $\hat{H}_{c.m.}|\Psi_g\rangle = E_g|\Psi_g\rangle$. The ground state $|\Psi_g\rangle$ can be written as a linear combination of the eigenstates of the Hamiltonian (23) as

$$|\Psi_g\rangle_{c.m.} = \sum_n \int_{-\infty}^{\infty} dk_2 \langle n, k_2|\Psi_g\rangle_{c.m.}|n, k_2\rangle, \qquad (C3)$$

where we have used the completeness relation for the eigenstates ($|n, k_2\rangle = |n\rangle \otimes |k_2\rangle$) of the Hamiltonian (23) for the system without potential along $\hat{x}_2$.

When we transform the ground state $|\Psi_g\rangle_{c.m.}$ using the unitary operator $\hat{U}$, the operator $\hat{U}$ introduces a superposition of displaced number states [109,110]. Specifically, this can be expressed as $|\alpha, n\rangle = \hat{U}|n, k\rangle = e^{\alpha(\hat{a}_1^\dagger - \hat{a}_1)}|n\rangle \otimes |k_2\rangle$, where α is a parameter associated with displacement [as discussed in

(36) for $n = 0$]. This transformation indicates that including a potential in the x_2 direction generally disrupts the coherent superposition of classical (coherent) states. However, to realize catlike states, it is essential to have a superposition of two diametrically opposite coherent states. Thus, to demonstrate the natural emergence of these catlike states, we consider the harmonic potential to depend solely on $\hat{x}_1$.

Furthermore, if we consider the situation where the negatively charged particle is also attached to a harmonic trap potential in the y_1 direction, the system Hamiltonian can be expressed as

$$\tilde{H}_{NC} = \frac{\hat{P}_1^2}{2m_B} + \frac{\hat{P}_2^2}{2m_B} + V_1(\hat{x}_1) + V_2(\hat{y}_1), \qquad (C4)$$

where $V_1(\hat{x}_1)$ and $V_2(\hat{y}_1)$ are oscillatory potentials. To focus on the basic situation, we do not write them explicitly.

Using the fact of (13), we can eliminate the degrees of freedom of the second charged particle in terms of the phase-space variables of the first charged particle as $\hat{y}_1 = \hat{x}_1 + \frac{c}{eB}\hat{P}_2$, and the above Hamiltonian can be rewritten as

$$\tilde{H}_{NC} = \hat{U}\tilde{H}_{c.m.}\hat{U}^\dagger, \qquad (C5)$$

with

$$\tilde{H}_{c.m.} = \frac{\hat{P}_1^2}{2m_B} + \frac{\hat{P}_2^2}{2m_B} + V_1(\hat{R}_1) + V_2\left(\hat{R}_1 + \frac{c}{eB}\hat{P}_2\right). \quad (C6)$$

The structure of the Hamiltonian (C6) clearly indicates that the introduction of a potential associated with the second charged particle in the $\hat{y}_1$ direction effectively induces a coupling between $\hat{P}_2$ and $\hat{R}_1$. This is quite similar to the case of Hamiltonian (C2). Following the same logic applied to the case for the positively charged particle also trapped by the potential in the $\hat{x}_2$ direction, we can immediately conclude that the feature of the catlike state will not be exhibited if we allow the potential for the second negatively charged particle in the $\hat{y}_1$ direction along with the potential attached to the first positively charged particle in the $\hat{x}_1$ direction. Therefore, for simplicity and clarity in our analysis focused on the positively charged particle, we restrict the harmonic potential V to depend solely on x_1.

[1] W. H. Zurek, Decoherence and the transition from quantum to classical, Phys. Today **44**(10), 36 (1991); *Quantum Theory of Measurement*, edited by J. A. Wheeler and W. H. Zurek (Princeton University Press, Princeton, 1983), pp. 152–167.

[2] S. Haroche and D. Kleppner, Cavity quantum electrodynamics, Phys. Today **42**(1), 24 (1989).

[3] E. Schrödinger, Naturwissenschaften **23**, 844 (1935).

[4] A. J. Leggett, Schrödinger's cat and her laboratory cousins, Contemp. Phys. **25**, 583 (1984).

[5] C. C. Gerry and P. L. Knight, Quantum superpositions and Schrödinger cat states in quantum optics, Am. J. Phys. **65**, 964 (1997).

[6] R. Penrose, On gravity's role in quantum state reduction, Gen. Relativ. Gravit. **28**, 581 (1996).

[7] A. Vinante, R. Mezzena, P. Falferi, M. Carlesso, and A. Bassi, Improved noninterferometric test of collapse models using ultracold cantilevers, Phys. Rev. Lett. **119**, 110401 (2017).

[8] B. Helou, B. J. J. Slagmolen, D. E. McClelland, and Y. Chen, LISA pathfinder appreciably constrains collapse models, Phys. Rev. D **95**, 084054 (2017).

[9] A. Bassi, K. Lochan, S. Satin, T. P. Singh, and H. Ulbricht, Models of wave-function collapse, underlying theories, and experimental tests, Rev. Mod. Phys. **85**, 471 (2013).

[10] H. J. Kimble, M. Dagenais, and L. Mandel, Photon antibunching in resonance fluorescence, Phys. Rev. Lett. **39**, 691 (1977).

[11] R. Short and L. Mandel, Observation of sub-Poissonian photon statistics, Phys. Rev. Lett. **51**, 384 (1983).

[12] R. E. Slusher, L. W. Hollberg, B. Yurke, J. C. Mertz, and J. F. Valley, Observation of squeezed states generated by four-wave mixing in an optical cavity, Phys. Rev. Lett. **55**, 2409 (1985).

[13] M. A. Nielsen and I. L. Chuang, *Quantum Computation and Quantum Information* (Cambridge University Press, Cambridge, 2009).

[14] *The Physics of Quantum Information: Quantum Cryptography, Quantum Teleportation, Quantum Computation*, edited by D. Bouwmeester, A. Ekert, and A. Zeilinger (Springer, Berlin, 2000).

[15] A. Gilchrist, K. Nemoto, W. J. Munro, T. C. Ralph, S. Glancy, S. L. Braunstein, and G. J. Milburn, Schrödinger cats and their power for quantum information processing, J. Opt. B **6**, S828 (2004).

[16] K. Gietka, Squeezing by critical speeding up: Applications in quantum metrology, Phys. Rev. A **105**, 042620 (2022).

[17] D. Hung, R. Malaney, and J. Green, Teleportation of a Schrödinger's-Cat state via satellite-based quantum communications, in *IEEE Globecom Workshops (GC Wkshps), Waikoloa, USA* (IEEE, Piscataway, NJ, 2019), pp. 1–5.

[18] D. S. Schlegel, F. Minganti, and V. Savona, Quantum error correction using squeezed Schrödinger cat states, Phys. Rev. A **106**, 022431 (2022).

[19] J. Hastrup and U. L. Andersen, All-optical cat-code quantum error correction, Phys. Rev. Res. **4**, 043065 (2022).

[20] W. Schleich, J. P. Dowling, R. J. Horowicz, and S. Varro, in *New Frontiers in Quantum Optics and Quantum Electrodynamics*, edited by A. Barut (Plenum, New York, 1990).

[21] The notion of interference between macroscopically distinguishable states has been promoted most prominently by A. Leggett, in *Proceedings of the Internal Symposium on Foundations of Quantum Mechanics in the Light of New Technology*, edited by S. Kamefuchi (Physical Society of Japan, Tokyo, 1983).

[22] G. J. Milburn and D. F. Walls, Effect of dissipation on interference in phase space, Phys. Rev. A **38**, 1087 (1988).

[23] E. C. G. Sudarshan, Equivalence of semiclassical and quantum mechanical descriptions of statistical light beams, Phys. Rev. Lett. **10**, 277 (1963).

[24] M. Cosacchi, J. Wiercinski, T. Seidelmann, M. Cygorek, A. Vagov, D. E. Reiter, and V. M. Axt, On-demand generation of higher-order Fock states in quantum-dot-cavity systems, Phys. Rev. Res. **2**, 033489 (2020).

[25] C. Navau, S. Minniberger, M. Trupke, and A. Sanchez, Levitation of superconducting microrings for quantum magnetomechanics, Phys. Rev. B **103**, 174436 (2021).

[26] B. Li, W. Qin, Y. F. Jiao, C. L. Zhai, X. W. Xu, L. M. Kuang, and H. Jing, Optomechanical Schrödinger cat states in a cavity Bose-Einstein condensate, Fund. Res. **3**, 15 (2023).

[27] J. Foo, R. B. Mann, and M. Zych, Schrödinger's cat for de Sitter spacetime, Class. Quantum Grav. **38**, 115010 (2021).

[28] C. Marletto and V. Vedral, Gravitationally induced entanglement between two massive particles is sufficient evidence of quantum effects in gravity, Phys. Rev. Lett. **119**, 240402 (2017).

[29] M. Christodoulou and C. Rovelli, On the possibility of laboratory evidence for quantum superposition of geometries, Phys. Lett. B **792**, 64 (2019).

[30] J.-Q. Liao, J.-F. Huang, and L. Tian, Generation of macroscopic Schrödinger-cat states in qubit-oscillator systems, Phys. Rev. A **93**, 033853 (2016).

[31] F.-X. Sun, S.-S. Zheng, Y. Xiao, Q. Gong, Q. He, and K. Xia, Remote generation of magnon Schrödinger cat state via magnon-photon entanglement, Phys. Rev. Lett. **127**, 087203 (2021).

[32] R. J. Marshman, S. Bose, A. Geraci, and A. Mazumdar, Entanglement of magnetically levitated massive Schrödinger cat states by induced dipole interaction, Phys. Rev. A **109**, L030401 (2024).

[33] S. Doplicher, K. Fredenhagen, and J. E. Roberts, The quantum structure of spacetime at the Planck scale and quantum fields, Commun. Math. Phys. **172**, 187 (1995); Spacetime quantization induced by classical gravity, Phys. Lett. B **331**, 39 (1994).

[34] H. Snyder, Quantized space-time, Phys. Rev. **71**, 38 (1947).

[35] A. Connes, Noncommutative geometry and reality, J. Math. Phys. **36**, 6194 (1995); R. Szabo, Quantum field theory on noncommutative spaces, Phys. Rep. **378**, 207 (2003); E. Akofor, A. P. Balachandran, and A. Joseph, Quantum fields on the Groenewold-Moyal plane, Int. J. Mod. Phys. A **23**, 1637 (2008).

[36] R. Banerjee, B. Chakraborty, S. Ghosh, P. Mukherjee and S. Samanta, Topics in noncommutative geometry inspired physics, Found. Phys. **39**, 1297 (2009).

[37] M. Chaichian, P. P. Kulish, K. Nishijima, and A. Tureanu, On a Lorentz-invariant interpretation of noncommutative spacetime and its implications on noncommutative QFT, Phys. Lett. B **604**, 98 (2004).

[38] S. M. Girvin, The quantum Hall effect: Novel excitations and broken symmetries, in *Topological Aspects of Low Dimensional Systems*, edited by A. Comtet, T. Jolicoeur, S. Ouvry, and F. David (Springer-Verlag, Berlin and Les Editions de Physique, Les Ulis, 2000); N. Macris and S. Ouvry, Projection on higher Landau levels and non-commutative geometry, J. Phys. A: Math. Gen. **35**, 4477 (2002).

[39] L. Susskind, The Quantum Hall fluid and noncommutative Chern-Simons theory, arXiv:hep-th/0101029.

[40] R. Jackiw and V. P. Nair, Relativistic wave equation for anyons, Phys. Rev. D **43**, 1933 (1991).

[41] N. Banerjee, R. Banerjee, and S. Ghosh, Relativistic theory of free anyon revisited, Phys. Rev. D **54**, 1719 (1996).

[42] H. Ishizuka and N. Nagaosa, Noncommutative quantum mechanics and skew scattering in ferromagnetic metals, Phys. Rev. B **96**, 165202 (2017).

[43] I. B. Pittaway and F. G. Scholtz, Quantum interference on the non-commutative plane and the quantum-to-classical transition, J. Phys. A: Math. Theor. **56**, 165303 (2023).

[44] D. Trinchero and F. G. Scholtz, Pinhole interference in three-dimensional fuzzy space, Ann. Phys. (NY) **450**, 169224 (2023).

[45] G. Amelino-Camelia, L. Doplicher, S. Nam, and Y.-S. Seo, Phenomenology of particle production and propagation in string-motivated canonical noncommutative spacetime, Phys. Rev. D **67**, 085008 (2003).

[46] I. Hinchliffe, N. Kersting, and Y. L. Ma, Review of the phenomenology of noncommutative geometry, Int. J. Mod. Phys. A **19**, 179 (2004).

[47] G. Amelino-Camelia, G. Mandanici, and K. Yoshida, On the IR/UV mixing and experimental limits on the parameters of canonical noncommutative spacetimes, J. High Energy Phys. 01 (2004) 037.

[48] Z. Dong and T. Senthil, Noncommutative field theory and composite Fermi liquids in some quantum Hall systems, Phys. Rev. B **102**, 205126 (2020).

[49] S. Hellerman and M. Van Raamsdonk, Quantum Hall physics = noncommutative field theory, J. High Energy Phys.10 (2001) 039.

[50] K. Cong, G. T. Noe II, and J. Kono, in *Encyclopedia of Modern Optics*, 2nd ed., edited by B. D. Guenther and D. Steel (Elsevier, Oxford, 2018), pp. 63–81.

[51] J. Gea-Banacloche, Collapse and revival of the state vector in the Jaynes-Cummings model: An example of state preparation by a quantum apparatus, Phys. Rev. Lett. **65**, 3385 (1990).

[52] Y. Ting and J. H. Eberly, Finite-time disentanglement via spontaneous emission, Phys. Rev. Lett. **93**, 140404 (2004).

[53] P. Saha, A. S. Majumdar, S. Singh, and N. Nayak, Collapse and revival of atomic entanglement in an intensity dependent Jaynes-Cummings interaction, Int. J. Quantum Inf. **08**, 1397 (2010).

[54] G. V. Dunne, R. Jackiw, and C. A. Trugenberger, "Topological" (Chern-Simons) quantum mechanics, Phys. Rev. D **41**, 661 (1990).

[55] D. Bigatti and L. Susskind, Magnetic fields, branes and noncommutative geometry, Phys. Rev. D **62**, 066004 (2000).

[56] P. Nandi, S. Sahu, and S. K. Pal, A note on broken dilatation symmetry in planar noncommutative theory, Nucl. Phys. B **971**, 115511 (2021).

[57] J. Zhou, W.-Y. Shan, W. Yao, and D. Xiao, Berry phase modification to the energy spectrum of excitons, Phys. Rev. Lett. **115**, 166803 (2015).

[58] A. Chernikov, T. C. Berkelbach, H. M. Hill, A. Rigosi, Y. Li, O. B. Aslan, D. R. Reichman, M. S. Hybertsen, and T. F. Heinz, Exciton binding energy and nonhydrogenic Rydberg series in monolayer WS$_2$, Phys. Rev. Lett. **113**, 076802 (2014).

[59] K. Cong, G. T. Noe II, and J. Kono, *Excitons in Magnetic Fields* (Elsevier, Oxford, 2018), pp. 63–81.

[60] E. Cobanera, P. Kristel, and C. Morais Smith, Quantum Brownian motion in a Landau level, Phys. Rev. B **93**, 245422 (2016).

[61] L. D. Faddeev and R. Jackiw, Hamiltonian reduction of unconstrained and constrained systems, Phys. Rev. Lett. **60**, 1692 (1988).

[62] R. Banerjee, H. J. Rothe, and K. D. Rothe, Hamiltonian approach to lagrangian gauge symmetries, Phys. Lett. B **463**, 248 (1999); R. Banerjee, The commutativity principle and Lagrangian symmetries, arXiv:hep-th/0001087.

[63] R. Jackiw, Physical instances of noncommuting coordinates, Nucl. Phys. B: Proc. Suppl. **108**, 30 (2002).

[64] J. S. Blakemore, Semiconducting and other major properties of gallium arsenide, J. Appl. Phys. **53**, R123 (1982).

[65] C. Cohen-Tannoudji, B. Diu, and F. Laloë, *Quantum Mechanics* (Hermann, Paris, 1977), Vol. 1.

[66] S. Biswas, P. Nandi, and B. Chakraborty, Emergence of a geometric phase shift in planar noncommutative quantum mechanics, Phys. Rev. A **102**, 022231 (2020).

[67] H. J. Rothe and K. D. Rothe, *Classical and Quantum Dynamics of Constrained Hamiltonian Systems* (World Scientific, Singapore, 2010).

[68] O. Bertolami, J. G. Rosa, C. M. L. de Aragao, P. Castorina, and D. Zappala, Noncommutative gravitational quantum well, Phys. Rev. D **72**, 025010 (2005).

[69] G. D. Barbosa and N. Pinto-Neto, Noncommutative quantum mechanics and Bohm's ontological interpretation, Phys. Rev. D **69**, 065014 (2004).

[70] G. D. Barbosa, On the meaning of the string-inspired noncommutativity and its implications, J. High Energy Phys. 05 (2003) 024.

[71] P. Basu, B. Chakraborty, and F. G. Scholtz, A unifying perspective on the Moyal and Voros products and their physical meanings, J. Phys. A: Math. Theor. **44**, 285204 (2011).

[72] W. M. Zhang, D. H. Feng, and R. Gilmore, Coherent states: Theory and some applications, Rev. Mod. Phys. **62**, 867 (1990).

[73] S. Mancini, D. Vitali, and P. Tombesi, Optomechanical cooling of a macroscopic oscillator by homodyne feedback, Phys. Rev. Lett. **80**, 688 (1998).

[74] R. L. de Matos Filho and W. Vogel, Even and odd coherent states of the motion of a trapped ion, Phys. Rev. Lett. **76**, 608 (1996).

[75] C. Gerry and P. L. Knight, *Introductory Quantum Optics* (Cambridge University Press, Cambridge, 2004).

[76] B. Yurke and D. Stoler, Generating quantum mechanical superpositions of macroscopically distinguishable states via amplitude dispersion, Phys. Rev. Lett. **57**, 13 (1986).

[77] A. Mecozzi and P. Tombesi, Distinguishable quantum states generated via nonlinear birefringence, Phys. Rev. Lett. **58**, 1055 (1987).

[78] M. W. Noel and C. R. Stroud, Jr., in *Coherence and Quantum Optics VII*, edited by J. Eberly, L. Mandel, and E. Wolf (Springer, New York, 1996), p. 563.

[79] J. Janszky, P. Domokos, and P. Adam, Coherent states on a circle and quantum interference, Phys. Rev. A **48**, 2213 (1993).

[80] R. Mirman, Analysis of the experimental meaning of coherent superposition and the nonexistence of superselection rules, Phys. Rev. D **1**, 3349 (1970).

[81] M. R. Dowling, S. D. Bartlett, T. Rudolph, and R. W. Spekkens, Observing a coherent superposition of an atom and a molecule, Phys. Rev. A **74**, 052113 (2006).

[82] B. Dutta Roy, in *Elements of Quantum Mechanics*, edited by D. Dutta Roy (New Age Science, Delhi, 2009).

[83] S. Bose, K. Jacobs, and P. L. Knight, Preparation of nonclassical states in cavities with a moving mirror, Phys. Rev. A **56**, 4175 (1997).

[84] G. Adesso, A. Serafini, and F. Illuminati, Entanglement, purity, and information entropies in continuous variable systems, Open Syst. Inf. Dyn. **12**, 189 (2005).

[85] L. S. Brown, Quantum motion in a Paul trap, Phys. Rev. Lett. **66**, 527 (1991).

[86] C. E. Crefeld and G. Platero, AC-driven localization in a two-electron quantum dot molecule, Phys. Rev. B **65**, 113304 (2002).

[87] H. Zeng, Quantum-state control in optical lattices, Phys. Rev. A **57**, 388 (1999).

[88] D. J. Thouless, Quantization of particle transport, Phys. Rev. B **27**, 6083 (1983).

[89] G. Burmeister and K. Maschke, Scattering by time-periodic potentials in one dimension and its influence on electronic transport, Phys. Rev. B **57**, 13050 (1998).

[90] W. Li and L. E. Reichl, Transport in strongly driven heterostructures and bound-state-induced dynamic resonances, Phys. Rev. B **62**, 8269 (2000).

[91] S. Das and G. S. Agarwal, Bright and dark periods in the entanglement dynamics of interacting qubits in contact with the environment, J. Phys. B **42**, 141003 (2009).

[92] Kh. P. Gnatenko, Parameters of noncommutativity in Lie-algebraic noncommutative space, Phys. Rev. D **99**, 026009 (2019).

[93] J. Shah, *Excitons in Semiconductor Nanostructures* (Springer, Berlin, 1999).

[94] E. J. Sie, J. W. McIver, Y.-H. Lee, L. Fu, J. Kong, and N. Gedik, Optical Stark effect in 2D semiconductors, Proc. SPIE Int. Soc. Opt. Eng. **9835**, 129 (2016).

[95] T. Mueller and E. Malic, Exciton physics and device application of two-dimensional transition metal dichalcogenide semiconductors, npj 2D Mater. Appl. **2**, 29 (2018).

[96] E. M. Lifshitz and L. P. Pitaevskii, *Statistical Physics*, 2nd ed. (Pergamon, Oxford, 1980), Pt. 2.

[97] S. A. E. Moskalenko, S. Moskalenko, and D. Snoke, *Bose-Einstein Condensation of Excitons and Biexcitons: and Coherent Nonlinear Optics with Excitons* (Cambridge University Press, Cambridge, 2000).

[98] A. Messiah, *Quantum Mechanics* (North-Holland, Amsterdam, 1962), Vol. 2.

[99] P. Nandi, B. R. Majhi, N. Debnath, and S. Kala, Quantum ballet by gravitational waves: Generating entanglement's dance of revival-collapse and memory within the quantum system, Phys. Lett. B **853**, 138706 (2024).

[100] G. Bir and G. Pikus, *Symmetry and Strain-Induced Effects in Semiconductors* (Wiley, New York, 1974).

[101] T.-C. Lu, Z. Zhang, S. Vijay, and T. H. Hsieh, Mixed-state long-range order and criticality from measurement and feedback, PRX Quantum **4**, 030318 (2023).

[102] A. Bhunia, M. K. Singh, M. A. Huwayz, M. Henini, and S. Datta, 0D-2D heterostructure for making very large quantum registers using 'itinerant' Bose-Einstein condensate of excitons, Mater. Today Electron. **4**, 100039 (2023).

[103] D. Xiao, J. Shi, and Q. Niu, Berry phase correction to electron density of states in solids, Phys. Rev. Lett. **95**, 137204 (2005).

[104] D. Xiao, M.-C. Chang, and Q. Niu, Berry phase effects on electronic properties, Rev. Mod. Phys. **82**, 1959 (2010).

[105] W. Yao and Q. Niu, Berry phase effect on the exciton transport and on the exciton Bose-Einstein condensate, Phys. Rev. Lett. **101**, 106401 (2008).

[106] A. A. Allocca, D. K. Efimkin, and V. M. Galitski, Fingerprints of Berry phases in the bulk exciton spectrum of a topological insulator, Phys. Rev. B **98**, 045430 (2018).

[107] P.-M. Ho and H.-C. Kao, Noncommutative quantum mechanics from noncommutative quantum field theory, Phys. Rev. Lett. **88**, 151602 (2002).

[108] B. Muthukumar and P. Mitra, Noncommutative oscillators and the commutative limit, Phys. Rev. D **66**, 027701 (2002).

[109] F. A. M. de Oliveira, M. S. Kim, P. L. Knight, and V. Bužek, Properties of displaced number states, Phys. Rev. A **41**, 2645 (1990).

[110] H. Goldman and T. Senthil, Lowest Landau level theory of the bosonic Jain states, Phys. Rev. B **105**, 075130 (2022).